2020 IEEE/RSJ International Conference on Intelligent Robots and Systems (IROS)
October 25-29, 2020, Las Vegas, NV, USA (Virtual)

Reliable chattering-free simulation of friction torque in joints presenting high stiction

Rafael Cisneros[1,*], Mehdi Benallegue[1], Ryo Kikuuwe[2], Mitsuharu Morisawa[1] and Fumio Kanehiro[1]

Abstract— **The simulation of static friction, and especially the effect of stiction, is cumbersome to perform in discrete-time due to its discontinuity at zero velocity and its switching behavior. However, it is essential to achieve reliable simulations of friction to develop compliant torque control algorithms, as they are much disturbed by this phenomenon. This paper takes as a base an elastoplastic model approach for friction, which is free from chattering and drift. It proposes two closed-form solutions that can be used to reliably simulate the effect of stiction consistently with the physics-based Stribeck model. These solutions consider the nonlinearity and velocity dependency, which are main characteristics of lubricated joints. One is directly inspired by the Stribeck nonlinear terms, and the other is a simplified rational approximation. The reliability of this simulation method is shown in simulation, where the consistency and stability are assessed. We also demonstrate the accuracy of these methods by comparing them to experimental data obtained from a robot joint equipped with a high gear reduction harmonic drive.**

Index Terms— **Joint friction simulation; Elasto-plastic friction model; Stiction**

I. Introduction

The use of dynamic simulation has undoubtedly sped up the development in robotics, especially in control. Through simulation, it is easier to predict and verify the behavior of control algorithms in the presence of unmodeled disturbances and nonlinearities, as well as to tune their parameters without compromising the integrity of the actual robot and the surroundings. Indeed, being robust to environment-related perturbations has gained relevance for robots designed to work on unstructured environments where collisions are likely. For this purpose, a joint torque control with compliance can safely cope with unexpected collisions by adapting to their geometry without generating high forces. Compliance can also guarantee more excellent safety when interacting with humans. However, the performance of such control schemes is greatly influenced by the presence of non-modeled joint friction. Many robotic systems commonly use servo-actuators with RV precision reduction gears [1] or harmonic drive gearing [2]. They are chosen for their absence of backlash and high gear ratios despite their small size. The drawback is their high level of friction.

Friction is a nonlinear phenomenon that is quite hard to model and not yet completely understood. It is a tangential reaction force between two surfaces in contact that is physically dependent on the load, geometry, topology, properties of the materials, relative velocity, and lubricant viscosity. Moreover, in robot joints, the complex interactions of gears, bearings, and shafts, which are rotating/sliding at different velocities, make physical modeling of the friction even more difficult [3] [4] [5]. The friction force always opposes the relative velocity of the surfaces in contact. When the velocity is zero, the friction force opposes other external forces to maintain zero velocity if the exerted force is below a threshold called static friction. This friction is the one that needs to be overcome to enable the relative motion of stationary objects in contact [6]. It is a regime of several microns of movement where the friction force is mainly a function of a pre-sliding displacement (before true sliding) [7]. This displacement arises due to elastic and plastic deformation of the contact asperities [8]. Stiction is the phenomenon that happens when the static friction is larger than the friction resulting during true sliding (i.e., kinetic friction) [9].

These effects undermine the quality of compliant joint torque control. While stiff actuation policies such as high gain position control suffer negligible impact from high stiction, the low-torque references from a compliant one are much disturbed. They generate erroneous joint accelerations, especially when initiating a motion.

One solution to tackle this problem is to use joint torque feedback to guarantee the tracking of torque references and compensate for frictions. However, joint torque sensors are costly, fragile, cumbersome, and heavy. Thus, they cannot be considered as a universal solution [10]. The other solution is to predict the friction torques and compensate for them in a feed-forward term. It is then necessary to simulate its effect on the robotic system as close as possible to reality.

Because of the above-mentioned complex nature of the friction, it is cumbersome to deal with zero velocity as it triggers a switching behavior, complicating its model in discrete-time. Therefore, most solutions for simulating this effect in discrete-time suffer from chattering [9].

Several models have been proposed to describe the friction and its associated phenomena, from simplistic models like the classic Coulomb model to others that can capture the nonlinearity and velocity dependency characteristic of lubricated joints following the observations of Stribeck [4]. Among these models, the ones that fall into the elastoplastic category can render static friction and pre-sliding displacement [11]. The model proposed by Kikuuwe et al. [9] lies in this category [12], as well as the model of Dupont et al. [11]. In particular, the model of Kikuuwe et al. proposes an implicit function transformation that applies to any characteristic friction function, and that allows for closed-form expressions

[1] CNRS-AIST JRL (Joint Robotics Laboratory), IRL, Tsukuba, Japan.
[2] Machinery Dynamics Lab., Hiroshima Univ., Higashi-Hiroshima, Japan.
[*] Corresponding author E-mail: rafael.cisneros@aist.go.jp

of the implicit Euler integration of discontinuous friction dynamics in discrete time. Furthermore, these expressions do not exhibit drift nor chattering, and are suitable for fixed-step computation, independently of the timestep [9]. However, with the method of Kikuuwe et al., it is not straightforward to find analytical solutions of the proposed implicit function transformation for all the friction functions. Thus, only a simple example is given in that paper (Coulomb + viscous friction) that does not consider the effect of stiction.

In this work, we take the idea of the implicit function transformation of [9] and apply it to two alternatives of complex friction functions that render the effect of stiction. In both cases, we were able to find closed-form solutions that allowed us to produce reliable simulations. This paper is organized as follows:

- Section II provides an overview of conventional friction models (and/or functions).
- Section III summarizes one of the improved elastoplastic friction models of Kikuuwe et al. [9]: the massless impedance-type model.
- Section IV develops the above-mentioned closed-form solutions to model the effect of stiction.
- Section V presents some experimental and simulation results that validate our models.
- Finally, Section VI concludes this paper.

II. Conventional friction models

Let us consider two surfaces in contact moving with relative velocity v while a tangential net force h is acting on them. The generated friction force f can be predicted by using a particular friction model. For simplicity, we assume that the sign of f is the opposite of v and h.

The most popular friction model is the classic Coulomb friction model, analytically expressed as

$$f = \begin{cases} h & \text{if } (v = 0) \,\&\, (|h| < F_S)\,, \\ F_S \mathrm{sgn}\,(h) & \text{if } (v = 0) \,\&\, (|h| \geq F_S)\,, \\ F_C \mathrm{sgn}\,(v) & \text{if } (v \neq 0)\,, \end{cases} \tag{1}$$

where $\mathrm{sgn}\,(\cdot)$ is the sign function, F_S is the static friction, and F_C is the Coulomb (kinetic) friction[1].

The previous model accounts for the effects of dry friction. However, servo-controlled machines are generally lubricated with oil or grease (hydrodynamic lubrication) [13]. In lubricated sliding contacts, the friction decreases with increased sliding speed until a mixed or full film situation is obtained. The friction in the contact can either be constant, increase, or decrease with the increased sliding speed due to viscous and thermal effect [14]. This behavior was described by Stribeck [4] such that for $v \neq 0$, we can write the friction model as

$$f = (F_S - F_C) \exp\left(- \left| \frac{v}{v_S} \right|^{\alpha} \right) \mathrm{sgn}\,(v) + F_C \mathrm{sgn}\,(v) + Dv, \tag{2}$$

[1]Actually, $F_S = \mu_S F_n$ and $F_C = \mu_C F_n$, where μ_S and μ_C are the corresponding friction coefficients and F_n is a normal force, but these details are omitted for simplicity.

where D is the coefficient of viscous friction, v_S is the break-away velocity, and α is the exponent of the Stribeck nonlinearity [5]. For $v = 0$ the behavior is described as in (1).

The main problem with the classical Coulomb model, or the Stribeck model, is that if used in the simulation, the condition $v = 0$ never occurs in discrete time. This situation leads to a chattering effect in which the friction force alternates between a positive and a negative value near to zero velocity. This effect prevents the simulated system from coming to a rest, contrary to what happens to the real machine. It is then common to define a small threshold value ϵ below which the velocity is considered zero, as suggested by Karnopp [15]. The problem is that the system's behavior is strongly influenced by choice of ϵ, which, by itself, does not have any physical meaning [9]. Furthermore, the behavior of the system at low velocities is not properly simulated.

The above-described models correspond to a non-physical simplification because real systems with distributed mass and compliance cannot exhibit an instantaneous change of force; that is, although they can render static friction, they do not deal with the pre-sliding displacement. An alternative strategy is regularizing these models with smoothing functions to replace the discontinuities. These functions can be linear, exponential, trigonometric or hyperbolic [7] [11]. For example, the sign function can be replaced by a saturation function or a hyperbolic tangent ($\tanh$) function. However, since the force is null at zero velocity, this strategy cannot reproduce static friction but adds computational stability.

Due to this trade-off, an alternative to the models based on the Coulomb is the models based on the bristle analogy: Within a given applied tangential load, the elastically deformed bristle returns to its original configuration after the tangential load is removed. These models are substantially different from the Coulomb approach, as they have continuous-time expressions based on differential equations. They involve an additional state that needs to be numerically integrated during the simulation. The most well-known model based on this analogy is the LuGre model [16], which is an extended version of the classical Dahl model [17]. However, these models do not adequately realize the static friction, i.e., they may result in unbounded drift even under external forces smaller than the maximum static friction force.

The elastoplastic model [18] [11] does realize static friction without causing unbounded drift, but one of its shortcomings is that it does not include the so-called micro-viscosity, i.e., the viscosity of the bristle, which prevents numerical oscillation in static friction. Kikuuwe et al.'s model [9] extends the elastoplastic model by considering the balance between the friction force and the visco-elastic force of the bristle in a particular differential-algebraic manner. Their model has been presented in an implicitly discretized form [9] and also in an Ordinary Differential Equation (ODE) form [19].

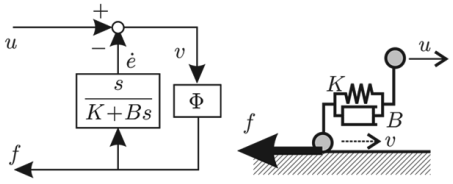

Fig. 1: Massless impedance-type friction model (Reprinted from Kikuuwe et al. (2006) [9]).

III. Improved elastoplastic friction model

In this section, we summarize the improved elastoplastic friction model proposed by Kikuuwe et al. (2006) [9]. Mainly, we describe the development of the massless impedance-type friction scheme described in that paper. This formalism is chattering-free and independent of the timestep.

Let us imagine that the contact interface between two surfaces consists of a virtual spring-damper, with spring constant $K > 0$ and damper constant $B > 0$, as illustrated in Fig. 1 [9]. This virtual spring-damper gives the relationship between two velocities: v and u, where u is the actual relative velocity and v is an auxiliary relative velocity.

The friction can be modeled by a friction function $\Phi(x)$ that (a) is continuous $\forall x \neq 0$, (b) satisfies $\Phi(x)\, x > 0\ \forall x \neq 0$ and (c) has limits as $x \to 0^+$ and $x \to 0^-$, namely $\Phi(+0)$ and $\Phi(-0)$ [9]. This allows us to consider several friction functions within this scheme capturing effects of interest of the friction phenomenon. In this way, the friction force f can be written as a function of the velocity v as

$$f = \Phi(v) \tag{3}$$

As illustrated in Fig. 1, we can also regard the friction force as a compliant element. In such a case, f is also given by

$$f = Ke + B\dot{e}, \tag{4}$$

with

$$\dot{e} = u - v. \tag{5}$$

Let us consider a discrete-time approximation with a timestep T, such that

$$\dot{e} \approx \frac{e_k - e_{k-1}}{T}. \tag{6}$$

Then, (3) and (4) can be discretized as

$$f_k = \Phi(v_k), \tag{7}$$

$$f_k = \frac{KT + B}{T} e_k - \frac{B}{T} e_{k-1}, \tag{8}$$

whereas from discretizing (5) we can obtain

$$e_k = (u_k - v_k)T + e_{k-1}. \tag{9}$$

By substituting (9) in (8) we get

$$v_k = u_k + \frac{Ke_{k-1}}{KT + B} - \frac{f_k}{KT + B}, \tag{10}$$

which can be substituted into (7) to obtain

$$f_k = \Phi(v_k^* - Zf_k), \tag{11}$$

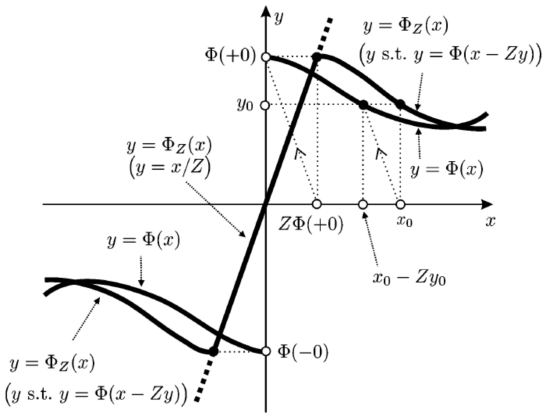

Fig. 2: Relationship between the friction function $\Phi(\cdot)$ and its implicit transformation $\Phi_Z(\cdot)$ (Reprinted from Kikuuwe et al. (2006) [9]).

with

$$Z = 1/(KT + B), \tag{12}$$

$$v_k^* = u_k + ZKe_{k-1}. \tag{13}$$

In [9], it is demonstrated that if $\Phi(x)$ satisfies the properties mentioned at the beginning of the section and also

$$\Phi'(x) = \frac{d}{dx}\Phi(x) > -1/Z \quad \forall x \neq 0, \tag{14}$$

then an implicit transformation function $\Phi_Z(x)$ exists s.t.

$$y = \Phi(x - Zy) \implies y = \Phi_Z(x) \tag{15}$$

holds true [9]. This function can be calculated as

$$\Phi_Z(x) = \begin{cases} y\ s.t.\ y = \Phi(x - Zy) & if\ x/Z \notin [\Phi(-0), \Phi(+0)], \\ x/Z & if\ x/Z \in [\Phi(-0), \Phi(+0)]. \end{cases} \tag{16}$$

The relationship between $\Phi(\cdot)$ and $\Phi_Z(\cdot)$ can be illustrated as in Fig. 2.

In this way, we can solve f_k in (11) as

$$f_k = \Phi_Z(v_k^*). \tag{17}$$

Here, v_k^* can be interpreted as the "hypothetical" velocity that could have been achieved if no friction force acted [9]; that is, $\Phi(\cdot)$ and $\Phi_Z(\cdot)$ are not supposed to act on the same velocity. Particularly, $\Phi_Z(\cdot)$ shall not be confused with a relaxation method of $\Phi(\cdot)$.

To simulate the friction force within our dynamics simulation framework we only need to follow Algorithm 1, which requires to update the error e_k once we have computed f_k. This can be done by solving (8) for e_k to get

$$e_k = Z(Be_{k-1} + f_k T), \tag{18}$$

where T is the simulation timestep.

The nonlinear algebraic equation in (16) cannot generally be solved analytically. However, for some simple cases, there are closed-form solutions [9]. For example, for Coulomb friction with viscous effect, we have

Algorithm 1 Simulation of friction force

$e_k \leftarrow 0$
while simulation is running **do**
  Read current system configuration
  $u_k \leftarrow$ current contact velocity
  $v_k^* \leftarrow u_k + ZKe_{k-1}$ (13)
  $f_k \leftarrow \Phi_Z(v_k^*)$ (17)
  Apply friction force to the system
  $e_k \leftarrow Z(Be_{k-1} + f_k T)$ (18)
end while

$$\Phi(x) = F\text{sgn}(x) + Dx, \tag{19}$$

where F is the dry friction, and D is the viscous friction coefficient. In this simple case, $\Phi_Z(x)$ becomes

$$\Phi_Z(x) = \begin{cases} \frac{F\text{sgn}(x)+Dx}{1+ZD} & \text{if } |x| > ZF, \\ x/Z & \text{if } |x| \leq ZF. \end{cases} \tag{20}$$

It is also worth mentioning that if the condition (14) is not respected, the resulting transformation becomes undefined, and the method will not work correctly. As seen in (12), Z depends on K and B, as well as on the friction function. So, we need to tune these model parameters having in mind the condition mentioned above.

IV. Friction models with stiction

In this section, we use the friction model described in Section III, which is able to render pre-sliding displacement, and propose two friction functions that can render the stiction. We show how to compute a closed-form solution for the implicit transformation function of each of them.

A. Stribeck friction function

Let us consider a friction function consistent with the Stribeck nonlinearity present in fluid-lubricated contacts and based on (2), for the case when the friction force increases with the increased relative velocity. By considering the nomenclature introduced in the last section, this friction function can be written as

$$\Phi(x) = F_{SC}\exp\left(-\left|\frac{x}{v_S}\right|^{\alpha}\right)\text{sgn}(x) + F_C\text{sgn}(x) + Dx, \tag{21}$$

where $F_{SC} = F_S - F_C$, $F_S > F_C > 0$, $D > 0$, $v_S > 0$, and $\alpha > 0$. This friction function is illustrated in Fig. 3.

For simplicity, we consider $\alpha = 1$. To calculate the implicit transformation function, we write $y = \Phi(x - Zy)$, obtaining

$$F_{SC}\text{sgn}(x - Zy) = \\ \left[-\left(F_C\text{sgn}(x - Zy) + Dx\right) + (1 + ZD)\, y\right]\exp\left(\left|\tfrac{x-Zy}{v_S}\right|\right). \tag{22}$$

Let us first evaluate the case $x > Zy$ to obtain one part of the solution of y, called y_+. This evaluation results in

$$F_{SC} = \left[-\left(F_C + Dx\right) + (1 + ZD)\, y_+\right]\exp\left(\frac{x - Zy_+}{v_S}\right). \tag{23}$$

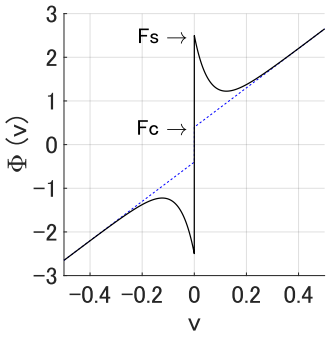

Fig. 3: Characteristic curve of the Stribeck friction model as a function of joint velocity v ($F_S = 2.5$ Nm, $F_C = 0.4$ Nm, $v_S = 0.06$ rad/s, $D = 4.5$ Nms/rad). Notice that F_C's meaning differs from the one for the classical Coulomb friction model described in (1).

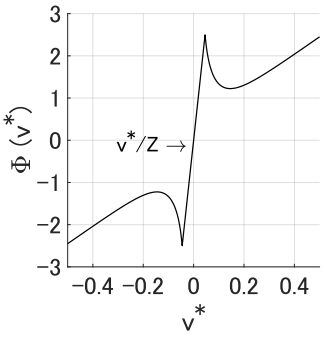

Fig. 4: Implicit transformation of the Stribeck friction function of Fig. 3, but written as function of the "hypothetical" joint velocity v^* ($K = 5000$ Nm/rad, $B = 50$ Nms/rad, $T = 0.001$ s).

To solve this equation for y_+ we first separate the exponential function; that is, as $\exp([x - Zy_+]/v_S) = \exp(x/v_S)\exp(-Zy_+/v_S)$. Then, we arrange the terms and multiply both sides of the equation by $-(Z/[v_S(1 + ZD)])$ to get

$$\psi_+ = w\exp(w), \tag{24}$$

with

$$\psi_+ = -\frac{Z}{v_S}\left(\frac{F_{SC}}{1 + ZD}\right)\exp\left(\frac{ZF_C - x}{v_S(1 + ZD)}\right), \tag{25}$$

$$w = \frac{Z}{v_S}\left(\frac{F_C + Dx}{1 + ZD}\right) - \frac{Z}{v_S}y_+. \tag{26}$$

It is possible to find a "closed-form" solution to (24) for y_+ if we make use of the Lambert W function, which is a multivalued inverse of the function $w \mapsto we^w$ [20]; that is, if $\psi = we^w$ then $w = W_k(\psi)$ where W_k is the Lambert W function and k specifies the required branch. This function can be solved fast and precisely with the method proposed by Fukushima [21]. For $\psi \in \mathbb{R}$ and $-1/e < \psi < 0$ there are two possible real values of the Lambert W function (see Fig. 5), or two branches: W_{-1} and W_0. The principal branch, W_0, satisfies $-1 \leq W(x)$.

We use the principal branch of the Lambert W function to solve (24) for y_+ such that $-1 < w$ holds as

$$y_+ = -\left(\frac{v_S}{Z}\right)W_0(\psi_+) + \frac{F_C + Dx}{1 + ZD}. \tag{27}$$

A similar procedure applies to the case $x < Zy$ to obtain the other part of the solution of y, called y_-. This case occurs when $x < 0$, which leads to

$$y_- = \left(\frac{v_S}{Z}\right)W_0(\psi_-) + \frac{-F_C + Dx}{1 + ZD}, \tag{28}$$

with

$$\psi_- = -\frac{Z}{v_S}\left(\frac{F_{SC}}{1+ZD}\right)\exp\left(\frac{ZF_C + x}{v_S\,(1+ZD)}\right). \tag{29}$$

Having obtained the two parts of the solution for y we can write $\Phi_Z(x)$ as

$$\Phi_Z(x) = \begin{cases} y_+ & \text{if } x > ZF_S, \\ x/Z & \text{if } |x| \le ZF_S, \\ y_- & \text{if } x < -ZF_S, \end{cases} \tag{30}$$

where y_+ and y_- are the solutions shown in (27) and (28), respectively.

The characteristic curve corresponding to (30) is shown in Fig. 4. Notice that it is plotted as a function of v^* instead of v to emphasize that it is not directly a function of the joint velocity, but a function of the "hypothetical" one as described in Section III.

For the characteristic curve of the implicit transformation function to be defined, the condition in (14) must be respected. When $x > 0$, $\Phi'(x)$ is given by

$$\Phi'(x) = -\frac{1}{v_S}F_{SC}\exp\left(-\frac{x}{v_S}\right) + D. \tag{31}$$

Due to the nature of the friction function we know that $\lim_{x\to 0}\Phi'(x) < \lim_{x\to\infty}\Phi'(x)$, or $-\frac{1}{v_S}F_{SC} + D < D$. Then, from (14), we have

$$\begin{aligned} &\Phi'(x) > -\frac{1}{v_S}F_{SC} + D > -\frac{1}{Z} \quad \forall x > 0, \\ &Z = \frac{1}{KT+B} \le \frac{v_S}{F_S} < \frac{v_S}{F_{SC}} < \frac{1}{\frac{1}{v_S}F_{SC} - D}. \end{aligned} \tag{32}$$

Because the robot joints are usually stiff, K should be as stiff as possible, but not stiffer than the harmonic drive transmission, in case there is one. However, a large K can make the simulation unstable, unless a smaller timestep T is considered. As for B, it is necessary to tune it to realize critical damping, provided that K and B meet (32). These parameters are normally chosen through trial and error [9].

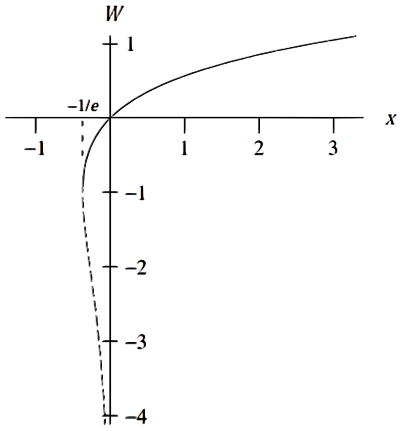

Fig. 5: The two real branches of the Lambert W function (Reprinted from Corless et al. (1996) [20]).

B. Simplified rational model

An alternative method to model the effect of the stiction is to use a rational friction model, written as

$$\Phi(x) = \begin{cases} \left(\gamma x^2 + \alpha x + \beta\right)/(x+\delta) & \text{if } x \ge 0, \\ -\left(\gamma x^2 - \alpha x + \beta\right)/(-x+\delta) & \text{if } x < 0 \end{cases} \tag{33}$$

Let us focus first on the right side plane of the function, for $x \ge 0$. The objective is to observe behavior like the one shown in Fig. 6. This behavior can be accomplished by imposing the following conditions:

$$\lim_{x\to\infty}\frac{\Phi(x)}{x} = D, \tag{34}$$

$$\lim_{x\to\infty}\Phi(x) - Dx = F_C, \tag{35}$$

$$\Phi(0) = F_S, \tag{36}$$

$$\Phi'(0) = -r, \tag{37}$$

with

$$r = \frac{F_S - F_C}{v_S} - D. \tag{38}$$

These conditions yield the following values for the coefficients of (33):

$$\gamma = D, \tag{39}$$

$$\delta = \frac{F_S - F_C}{r + D}, \tag{40}$$

$$\alpha = D\delta + F_C, \tag{41}$$

$$\beta = F_S\delta. \tag{42}$$

The resulting friction function is illustrated and compared with the Stribeck one in Fig. 7.

To calculate the implicit transformation function, we write $y = \Phi(x - Zy)$ as

$$y = \frac{\gamma(x-Zy)^2 + \alpha(x-Zy) + \beta}{x - Zy + \delta}. \tag{43}$$

By arranging terms, we can express the solution of y in the right side plane

$$y_+ = \left(-b_+ - \sqrt{b_+^2 - 4ac_+}\right)/(2a), \tag{44}$$

and, similarly, in the left side plane

$$y_- = \left(-b_- + \sqrt{b_-^2 - 4ac_-}\right)/(2a), \tag{45}$$

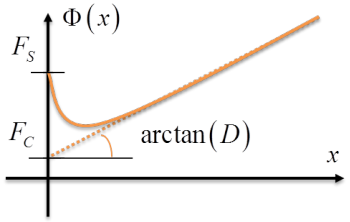

Fig. 6: Relationship between the parameters for the simplified rational model of friction and the shape of the function.

with

$$a = DZ^2 + Z, \tag{46}$$

$$b_\pm = -\left(\pm x + \delta \pm 2DZx + \alpha Z\right), \tag{47}$$

$$c_\pm = Dx^2 \pm \alpha x + \beta, \tag{48}$$

such that we can express $\Phi_Z(x)$ in the same way as in (30).

For the characteristic curve of the implicit transformation function to be defined, the condition in (14) must to be respected. We know that when $x > 0$, we also have $\lim_{x\to 0}\Phi'(x) < \lim_{x\to\infty}\Phi'(x)$, or $-r < D$ in this case. Then, from (14) we have

$$\begin{gathered}\Phi'(x) > -r > -\frac{1}{Z} \quad \forall x > 0, \\ r < KT + B = \frac{1}{Z}.\end{gathered} \tag{49}$$

To tune K and B, we can follow similar guidelines as in the previous model.

The characteristic curve corresponding to this implicit transformation function is also shown and compared with the Stribeck one in Fig. 8.

V. Experimental and Simulation Results

A. Hardware and control system description

To assess the validity of our models to simulate the static friction, and especially the stiction, we experimented on the right hand[2] of our humanoid robot HRP-5P (see Fig. 9) [22]. This robot's joints are driven are driven by high power electrical actuators, coupled to oil-lubricated Harmonic Drive Gears by pulleys and belts. As for the joints, there is no joint torque sensor. The servo only performs current control and, because of that, the friction effect is not compensated.

The simulations were performed using the dynamics simulator embedded in Choreonoid [23] using a simulation timestep $T = 1$ ms. This value was chosen to capture the dynamics of the robot. The connection of controllers to the robot is made by using the OpenRTM middleware system [24]. In this way, the reference torque is given to each joint of the robot. A "customizer" of the robot is used to simulate the effect of the friction. The "customizer" provides a pointer to the torques given to the joints and allows them to be modified. Notably, the friction torque was calculated and subtracted from the reference torque. Both approaches of friction that were proposed in this paper were implemented in this way. The Lambert W function used by the Stribeck approach was calculated using the implementation of Veberič [25][3]. However, calculating the Lambert W function is costly. So, we used it only to fill in a Look-Up-Table (LUT) that calculates only the first right-hand term of (27) up to some x for which this term becomes negligible. The first right-hand term of (28) can be calculated using the same LUT by considering symmetry. In this way, both approaches of friction resulted in similar computation times.

To control the joints, we used the inverse-dynamics-like control of [26], which uses a Quadratic Programming (QP) solver and a compensation term based on integral gains. We configured this controller to work only in joint-space; that is, we only considered a posture (configuration) task and no cartesian-space task. Furthermore, we didn't include any contact with the environment within the QP. As for the constraints, we only considered joint angle/velocity limits and torque limits for security reasons.

The posture task is implemented as a PD tracker with a feed-forward term to produce a joint acceleration reference $\ddot{q}_r$; that is,

$$\ddot{q}_r = k_p\left(q_d - q\right) + k_v\left(\dot{q}_d - \dot{q}\right) + \ddot{q}_d, \tag{50}$$

where k_p and k_v are PD gains, the subscript d indicates desired values, and variables without subscript refer to actual values. The joint acceleration reference $\ddot{q}_r$ is used to calculate the computed torque τ_c by using inverse dynamics. This computed torque is modified by an additional compensation term τ_p, calculated (for the case of the simple joint) as

[2]The rest of the joints of the robot were not powered during this test.

[3]Available at https://github.com/DarkoVeberic/LambertW.

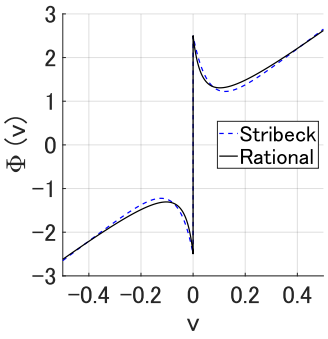

Fig. 7: Comparison between the rational function of friction and the Stribeck one of Fig. 3. The parameters of the former one were chosen to yield an equivalent curve ($F_S = 2.5$ Nm, $F_C = 0.2$ Nm, $v_S = 0.04$ rad/s, $D = 4.5$ Nms/rad).

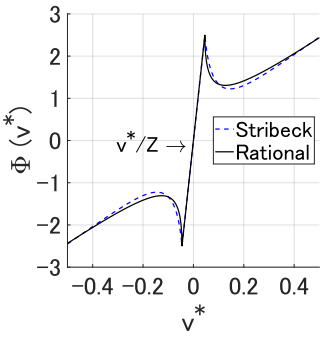

Fig. 8: Comparison between the implicit transformation of the rational friction function of Fig. 7 and the Stribeck one of Fig. 3 (both using $K = 5000$ Nm/rad, $B = 50$ Nms/rad, $T = 0.001$ s).

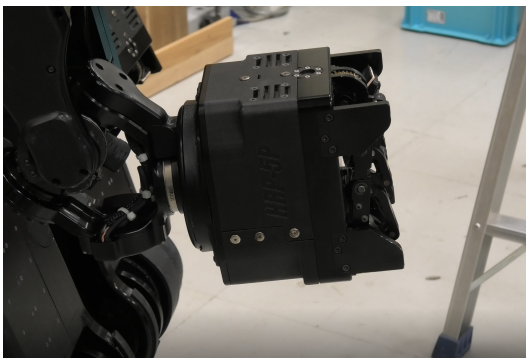

Fig. 9: Right hand's wrist joint of the HRP-5P robot [22].

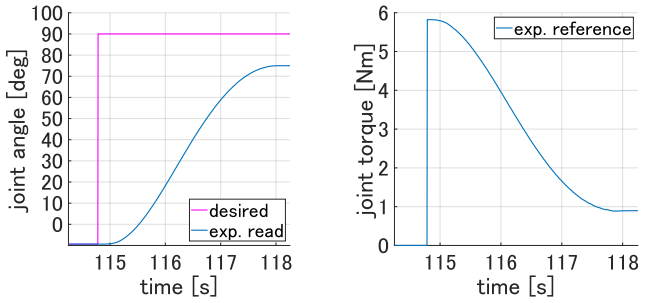

(a) Joint motion (b) Reference torque

Fig. 10: Experimental data without using an integral term.

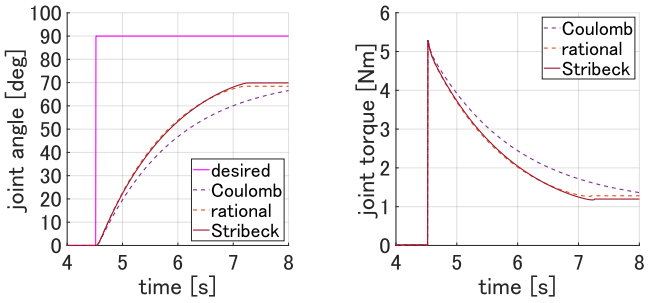

(a) Joint motion (b) Reference torque

Fig. 12: Simulation data without using an integral term.

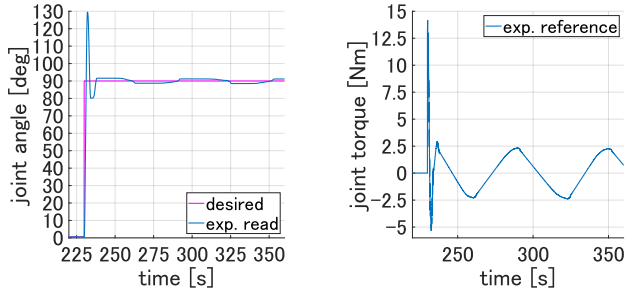

(a) Joint motion (b) Reference torque

Fig. 11: Experimental data when using the integral term.

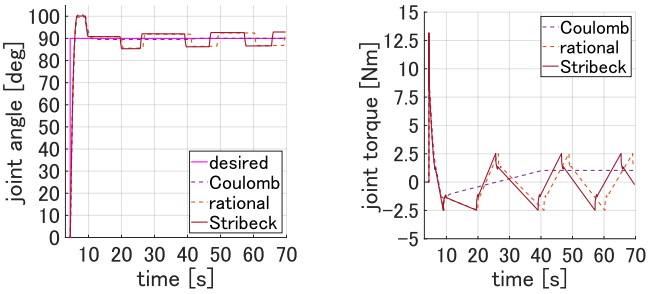

(a) Joint motion (b) Reference torque

Fig. 13: Simulation data when using the integral term.

$$\tau_p = K_I \left(\int \ddot{q}_r dt - \dot{q} \right), \tag{51}$$

with $K_I = \lambda M$, where $\lambda > 0$ and M is the joint's inertia. The reference torque $\tau_r = \tau_c + \tau_p$ is sent directly as a command to the joint servo.

B. Comparison of experimental and simulation results

As explained in Section I, our purpose is to implement a compliant torque control, realized by using low values for the PD gains in (50).

As a first test, we asked the joint to move from 0 deg to 90 deg using a step command and without using any integral compensation term. The PD gains that we used were $(k_p, k_v) = \left(20\ \mathrm{s}^{-2}, 2\ \mathrm{s}^{-1}\right)$. The resulting plots corresponding to the measured (read) joint angle and the reference torque are shown in Fig. 10. We can see that the initial torque is 5.8 Nm. This value is certainly larger than the static friction torque, as it was able to produce motion. Furthermore, we can see that the joint angle stops at 75 deg after 3.2 s as an effect of the kinetic friction torque when not using an integral compensation term. The reference torque becomes constant (0.9 Nm), but it does not produce motion as it would need to overcome the static friction once again.

Then, we turned on the integral compensation term, using $\lambda = 1\ \mathrm{s}^{-1}$ in (51). Also, the PD gains of the posture task were set to $(k_p, k_v) = \left(50\ \mathrm{s}^{-2}, 14\ \mathrm{s}^{-1}\right)$. The resulting plots corresponding to the measured (read) joint angle and the reference torque are shown in Fig. 11. We can see that the stiction prevents the actual joint value from reaching the desired one for small PD gains. We can observe a sawtooth-like plot for the torque produced by the integral term. This term linearly increases (or decreases) the torque when compensation is needed, with a slope that depends on the joint error, until reaching the static friction torque; that is, 2.5 Nm. At that moment, the actual joint value changes, but it crosses the desired one. Then, the joint velocity decreases until the reference torque is lower than the effective kinetic friction torque leading to a full stop of the joint motion.

From these experimental results, we heuristically tuned the friction parameters of both of the functions proposed in this paper: Stribeck and rational. The resulting parameters are the same ones used to generate the plots of Fig. 4 and Fig. 8. Additionally, for the effect of comparison, we tuned the friction parameters of the simple Coulomb function with the viscous effect defined in (19), which does not consider stiction. We used $F = 1.0$ Nm and $D = 4.5$ Nms/rad for this latter case.

The simulation results for the case that uses no integral term are shown in Fig. 12. As we can see, the behavior is quite similar when using the Stribeck and the rational function, although the joint motion stops abruptly a little earlier than in the experiment: at 69.9 deg or 68.4 deg, respectively. In both cases, the joint motion seemed faster than in the experiment (2.75 s), probably because the viscous friction coefficient has a higher effect on lower velocities; that is, the experimental viscous friction might not be linear. As for the Coulomb function, we can see that the motion is slower and approaches asymptotically towards an angle around 70 deg.

The simulation results for the case that uses the integral term are shown in Fig. 13. Here, we can see that both the Stribeck and the rational function capture the sawtooth-like behavior seen in the experiment, although its frequency is different (notice that the scale of the time axis is not the same). This difference is because the oscillation depends on how close the joint motion stops to the desired angle. Also, we notice that the joint motion overshoot of the experiment was not captured in the same way. These behaviors depend on additional characteristics of the friction not yet considered: the nonlinearity of the viscous friction and hysteresis. As for the Coulomb function, we can see that it behaves entirely different, as the joint converges to the desired angle (90 deg) with zero static error, due to the effect of the integral term. This difference in behavior justifies the necessity of our proposed models.

It is worth emphasizing that our target is not to identify the best friction force parameters of our specific joints. It is a complicated problem requiring to model a large number of parameters. We just aim to produce stable simulations to predict the effect of the friction on a control policy.

VI. Conclusion and future work

This paper developed two alternative solutions to reliably simulate the effect of the stiction without introducing numerical instability. In both cases, it was possible to broadly resemble the behavior observed while testing compliant control laws on a real joint of our robot. Minor details, like the bigger overshoot amplitude of the experiment considering the integral term, require additional friction dynamics that are beyond the scope of the proposed solutions.

Concerning the computational cost, although the Stribeck-inspired solution can be very costly if directly implemented (due to the computation of the Lambert W function), it is possible to achieve the same efficiency as the rational solution by considering the use of a Look-Up-Table.

Another issue to consider is tuning both solutions to behave similarly. If the stiction is larger than the case presented in the paper, it may not be possible to match the behavior simultaneously at low and high velocities, and a trade-off might have to be considered. On the other hand, it seems that in any case, it is not worth to precisely tune the friction parameters, as we found that they change in the real system according to various parameters such as time and temperature. It is more important to achieve a good simulation of the rough stiction effect on the system dynamics to design a robust compensation algorithm.

As future work, we want to include the effect of the above-mentioned additional friction dynamics, namely hysteresis, and nonlinear viscous effect. We want to use this simulation scheme to design a feed-forward friction-compensation torque to overcome the effect of stiction and realize a well-behaved, compliant torque control.

Acknowledgments

This work was partially supported by NEDO's "Development of a highly dependable humanoid robot system that can work in unstructured environments" project.

References

[1] K. Yokoji and M. Saito, "A challenging problem : the dynamic analysis of a high precision reduction gear," in *SIMULIA Customer Conf.*, 2010.

[2] J. Hauschild, G. Heppler, and J. McPhee, "Friction Compensation of Harmonic Drive Actuators," in *Int. Conf. on Dynamics and Control of Systems and Structures in Space (DYCOSS)*, 2004.

[3] C. Canudas-de-Wit, H. Olsson *et al.*, "A new model for control of systems with friction," *IEEE Trans. on Automatic Control*, vol. 40, no. 3, 1995.

[4] B. Jacobson, "The Stribeck memorial lecture," *Tribology International*, vol. 36, no. 11, 2003.

[5] A. C. Bittencourt and S. Gunnarsson, "Static Friction in a Robot Joint - Modeling and Identification of Load and Temperature Effects," *Journal of Dynamic Systems, Measurement, and Control*, vol. 134, no. 5, 2012.

[6] J. A. Munoz, D. E. Nikonov *et al.*, "Magnetic nanomechanical devices for stiction compensation," U.S. Patent US9 926 193B2, 2018. [Online]. Available: https://patents.google.com/patent/US9926193B2/en

[7] E. Pennestrì, V. Rossi *et al.*, "Review and comparison of dry friction force models," *Nonlinear Dynamics*, vol. 83, no. 4, 2015.

[8] B. Armstrong and C. Canudas-de-Wit, *The Control Handbook, Volume I*, 1st ed., ser. Electric Engineering Handbook. CRC-Press, 1996, ch. Friction Modeling and Compensation.

[9] R. Kikuuwe, N. Takesue *et al.*, "Admittance and Impedance Representations of Friction Based on Implicit Euler Integration," *IEEE Trans. on Robotics*, vol. 22, no. 6, 2006.

[10] G. Morel and S. Dubowsky, "The Precise Control Of Manipulators With Joint Friction: A Base Force/Torque Sensor Method," in *IEEE Int. Conf. on Robotics and Automation (ICRA*, 1996.

[11] P. Dupont, B. Armstrong, and V. Hayward, "Elasto-Plastic Friction Model: Contact Compliance and Stiction," in *American Control Conference (ACC)*, 2000.

[12] M. Iwatani and R. Kikuuwe, "Some Improvements in Elastoplastic Friction Compensator," *SICE Journal of Control, Measurement, and System Integration*, vol. 10, no. 3, pp. 141–148, 2017.

[13] L. Márton and N. Kutasi, "Practical Identification Method for Striebeck Friction," in *Int. Symp. of Hungarian Researchers*, 2005.

[14] S. Andersson, A. Söderberg, and S. Björklund, "Friction models for sliding dry, boundary and mixed lubricated contacts," *Tribology International*, vol. 40, no. 4, 2007.

[15] D. Karnopp, "Computer Simulation of Stick-Slip Friction in Mechanical Dynamic Systems," *Journal of Dynamics, Systems, Measurement, and Control*, vol. 107, no. 1, 1985.

[16] K. J. Åström and C. Canudas-de-Wit, "Revisiting the LuGre Friction Model: Stick-Slip Motion and Rate Dependence," *IEEE Control Systems Magazine*, vol. 28, no. 6, 2008.

[17] P. R. Dahl, "Solid friction damping of mechanical vibrations," *American Institute of Aeronautics and Astronautics (AIAA) Journal*, vol. 14, no. 12, 1976.

[18] V. Hayward and B. Armstrong, "A new computational model of friction applied to haptic rendering," in *Experimental Robotics VI*, ser. Lecture Notes in Control and Information Sciences, P. Corke and J. Trevelyan, Eds. Springer-Verlag, 2000, vol. 250.

[19] X. Xiong, R. Kikuuwe, and M. Yamamoto, "A differential algebraic method to approximate nonsmooth mechanical systems by ordinary differential equations," *Journal of Applied Mathematics*, 2013.

[20] R. M. Corless, G. H. Gonnet *et al.*, "On the Lambert W Function," *Advances in Computational Mathematics*, vol. 5, 1996.

[21] T. Fukushima, "Precise and fast computation of Lambert W-functions without transcendental function evaluations," *Journal of Computational and Applied Mathematics*, vol. 244, no. 1, 2013.

[22] K. Kaneko, H. Kaminaga *et al.*, "Humanoid Robot HRP-5P: an Electrically Actuated Humanoid Robot with High Power and Wide Range Joints," *IEEE Robotics and Automation Letters (RA-L)*, vol. 4, no. 2, 2019.

[23] S. Nakaoka, "Choreonoid: Extensible Virtual Robot Environment Built on an Integrated GUI Framework," in *IEEE/SICE Int. Symp. on System Integration (SII)*, 2012.

[24] N. Ando, T. Suehiro *et al.*, "RT-Middleware: Distributed Component Middleware for RT (Robot Technology)," in *IEEE/RSJ Int. Conf. on Intelligent Robots and Systems (IROS)*, 2005.

[25] D. Veberič, "Lambert W Function for Applications in Physics," *Computer Physics Communications*, vol. 183, no. 12, 2012.

[26] R. Cisneros, M. Benallegue *et al.*, "Robust humanoid control using a QP solver with integral gains," in *IEEE/RSJ Int. Conf. on Intelligent Robots and Systems (IROS)*, 2018.